Voltage control of magnetic single domains in Ni discs on ferroelectric $BaTiO_3$

M. Ghidini[1,2,3*], B. Zhu[3], R. Mansell[4,#], R. Pellicelli[5], A. Lesaine[3], X. Moya[3], S. Crossley[3], B. Nair[3], F. Maccherozzi[2], C. H. W. Barnes[4], R. P. Cowburn[4], S. S. Dhesi[2] and N. D. Mathur[3,†]

[1] Department of Mathematics, Physics and Computer Science, University of Parma, 43124 Parma, Italy

[2] Diamond Light Source, Chilton, Didcot, Oxfordshire, OX11 0DE, UK

[3] Department of Materials Science, University of Cambridge, Cambridge, CB3 0FS, UK

[4] Cavendish Laboratory, University of Cambridge, CB3 0HE, UK

[5] Istituto d'Istruzione Superiore A. Zanelli, 42123 Reggio Emilia, Italy

Now at NanoSpin, Department of Applied Physics, Aalto University, FI-00076 Aalto, Finland

* massimo.ghidini@fis.unipr.it

† ndm12@cam.ac.uk

For 1 μm-diameter Ni discs on a $BaTiO_3$ substrate, the local magnetization direction is determined by ferroelectric domain orientation as a consequence of growth strain, such that single-domain discs lie on single ferroelectric domains. On applying a voltage across the substrate, ferroelectric domain switching yields non-volatile magnetization rotations of 90°, while piezoelectric effects that are small and continuous yield non-volatile magnetization reversals that are non-deterministic. This demonstration of magnetization reversal without ferroelectric domain switching implies reduced fatigue, and therefore represents a step towards applications.

Ferroelectric and ferromagnetic materials that are coupled via strain or exchange bias show large magnetoelectric effects at room temperature, and have therefore attracted considerable interest since the turn of the century [1-5]. For example, the heterostructures that display these magnetoelectric effects permit an applied electric field to switch individual magnetic domains [6], modify a large in-plane magnetization [7-8], switch a large magnetization from

out-of-plane to in-plane [9], reorient magnetic easy axes [10], modulate coercivity [11], and control magnetic domain wall motion [12].

Despite the aforementioned interest, there have been very few studies of magnetoelectric heterostructures in which the active regions are patterned and not continuous [13]. Studies of patterned magnetoelectric heterostructures are scientifically interesting, because the resulting lateral magnetic confinement is known to produce a variety of exotic ground states [14], whose response to electrically driven changes of strain/exchange bias has barely been studied. For example, electrically driven strain can modify Landau flux closure structures [15], and switch the chirality of a magnetic vortex [16] or a magnetic vortex wall [17]. Studies of patterned magnetoelectric heterostructures are also attractive because of the technological promise of low-power memory applications [13]. This might involve the electrical manipulation of a magnetic single domain (SD), which has rarely been achieved [18], and not achieved with vector maps of in-plane magnetization or concomitant ferroelectric domain imaging.

Here we demonstrate magnetoelectric effects in 10 nm-thick polycrystalline discs of Ni, which are typically SD when they lie on a single ferroelectric domain of the single-crystal $BaTiO_3$ (BTO) substrate that we employ. The 1 μm disc diameter exceeds the 400 nm critical diameter for a SD of this thickness [19], but the virgin SD state is stabilized by a tensile growth strain that lies along the *c* axis [20]. (By contrast, thicker films of polycrystalline Ni experience isotropic tensile growth strains on all substrates [9].) As a consequence of the uniaxial tensile growth strain here, disc magnetization decorates the underlying ferroelectric domains, just as the magnetization of a polycrystalline CoFe film decorates the ferroelectric domains in its BTO substrate [20]. Our magnetoelectric effects are mediated by electrically induced strains that are large enough to overcome the growth strain, such that they also stabilize SDs.

Disc magnetization was imaged using photoemission electron microscopy (PEEM) with contrast from X-ray magnetic circular dichroism (XMCD), whereas the ferroelectric domains were imaged using PEEM with contrast from X-ray linear dichroism (XLD). After imaging with PEEM, disc magnetization was imaged using magnetic force microscopy (MFM), and the ferroelectric domains were imaged using optical birefringence. In our magnetoelectric

experiments, the magnetization of SD discs was electrically controlled in two ways. First, via large strains from ferroelectric domain switching, which produced non-volatile magnetization rotations of 90°. Second, via small and continuous piezoelectric effects, which produced volatile magnetization rotations of 90° that on voltage removal resulted in non-volatile magnetization reversals, which we infer to be non-deterministic. In our analysis, micromagnetic simulations were used to quantify the strain required to stabilize the SD state in our Ni discs. This led us to identify a suppression of saturation magnetization with respect to bulk Ni.

Experimental methods

A 0.5 mm-thick BTO substrate in the pseudo-cubic (001) orientation, with a 200 nm-thick pre-sputtered back electrode of Pt, was cleaned in ultrasound using acetone, IPA and DI water, sequentially. Next, we used thermal evaporation to deposit a 2 nm-thick top electrode of Al, on which we spun a double layer of PMMA resist (100 K A6 /495 K A4). This resist was patterned using e-beam lithography to define 10×10 arrays of 1 μm-diameter discs, whose centres were separated by 2 μm. After using e-beam sources in an MBE system (base pressure 3×10^{-10} mbar) to grow 10 nm of Ni capped with 3 nm of Cu, we performed lift-off in acetone to produce the sample shown schematically in Fig. 1a.

PEEM was performed with the X-ray beam at a grazing-incidence angle of 16°, using an Elmitec SPELEEM-III microscope on beamline I06 at Diamond Light Source, and a 300 V power supply that was connected to the sample via feedthroughs in the holder. The probe depth was ~7 nm, and the lateral resolution was typically ~50 nm. Images of ferromagnetic (ferroelectric) domains without topographical information were obtained by plotting average values of XMCD (XLD) asymmetry. These values represent the projection onto the incident-beam direction of the local surface magnetization (polarization). For images acquired with right (R) and left (L) circularly polarized light, the XMCD asymmetry of each pixel is given by $\left(I^{\mathrm{R}}-I^{\mathrm{L}}\right)/\left(I^{\mathrm{R}}+I^{\mathrm{L}}\right)$, where $I^{\mathrm{R/L}}=\left(I_{\mathrm{on}}^{\mathrm{R/L}}-I_{\mathrm{off}}^{\mathrm{R/L}}\right)/I_{\mathrm{off}}^{\mathrm{R/L}}$ is the relative intensity for secondary electron emission arising from X-ray absorption on ($I_{\mathrm{on}}^{\mathrm{R/L}}$ at 851 eV) and off ($I_{\mathrm{off}}^{\mathrm{R/L}}$ at 842 eV) the Ni L_3 resonance. For images acquired with light that is polarized vertically (V) and horizontally (H) with respect to the sample surface, the XLD asymmetry of each pixel is given by $\left(I^{\mathrm{V}}-I^{\mathrm{H}}\right)/\left(I^{\mathrm{V}}+I^{\mathrm{H}}\right)$, where $I^{\mathrm{V/H}}=\left(I_{\mathrm{on}}^{\mathrm{V/H}}-I_{\mathrm{off}}^{\mathrm{V/H}}\right)/I_{\mathrm{off}}^{\mathrm{V/H}}$ is the relative intensity for

secondary-electron emission arising from X-ray absorption on ($I_{on}^{V/H}$ at 457 eV) and off ($I_{off}^{V/H}$ at 446 eV) the Ti L_3 resonance. The comparison between intensities obtained on and off resonance avoids the influence of any inhomogeneous illumination. Images for each X-ray energy and beam polarization were acquired during 1 s exposure times. Each PEEM image was constructed via an averaging process based on 40 such images. Maps of the local in-plane magnetisation were calculated by vectorially combining for each pixel the XMCD asymmetry from two images obtained using orthogonal in-plane projections of the incident-beam direction. Drift and distortion were corrected via an affine transformation that matched the two topographic X-ray absorption images.

MFM was performed using a Digital Instruments Dimension 3100, at lift heights of 40-60 nm, using low-moment ASYMFMLM Asylum Research tips of stiffness 2 N m^{-1} that were coated with 15 nm of CoCr. The image analysis was performed using Gwyddion [21]. The MFM contrast from our discs was in the dipolar regime [14], and there was negligible tip-sample interaction given that a reversal of tip magnetization produced contrast inversion (not shown). SDs were identified when we observed the stray field associated with a single magnetic dipole.

Micromagnetic simulations were performed using MuMax3, an open-source micromagnetic simulation package [22]. A Ni disc of diameter 1 μm and thickness 10 nm was discretized into cells of 5×5×2 nm^3. The exchange stiffness was taken to be 0.82×10^{-11} J m^{-1} [23]. Uniaxial strain ε_y from the substrate was assumed to introduce a magnetic stress anisotropy energy of density $-K\cos^2\theta$, where θ is the angle between the magnetization and the strain axis parallel to y, $K = \frac{3}{2} E\varepsilon_y\lambda$, Young's modulus $E = 133$ GPa, and Ni magnetostriction $\lambda = -32.9\times10^{-6}$ [9]. Stable equilibrium configurations were found by dynamically relaxing the magnetization, and performing a minimization using the conjugate gradient method. The phase diagram that we show later was obtained by writing and compiling a Go program that directly utilizes calls to functions of MuMax3.

Optical microscopy was carried out using an Olympus BH microscope in reflection mode, with an unpolarized light source and an analyzer. Images were captured using a Moticam 1000 camera. Ferroelectric domain structures were established by observing the image contrast while rotating the analyser. For BTO, the ordinary refractive index exceeds the

extraordinary refractive index, such that the Fresnel equations predict a lower reflectivity for light polarized along the optic axis (the *c* axis) than light polarized along an orthogonal axis (an *a* axis). Therefore domains appeared dark when the analyzer was aligned with the ferroelectric polarization.

Results

Starting with the virgin sample, we used XMCD-PEEM to image part of a 10×10 array of Ni discs through the 3 nm Cu caps (Fig. 1a), and we used XLD-PEEM to image the surrounding ferroelectric domains through the 2 nm Al capping layer that serves as the upper electrode. By combining the two images (Fig. 1b), we find that discs decorate ferroelectric domains that are separated by walls oriented at 45° degrees to the axes of the disc array. Any part of a disc that is associated with a dark ferroelectric domain possesses a relatively large XMCD asymmetry, implying that the local magnetization lies approximately parallel (white) or antiparallel (black) to the in-plane projection of the incident X-ray beam direction (green arrow, Fig. 1b). Therefore discs lying wholly within dark ferroelectric domains are inferred to be SD. Any part of a disc that is associated with a bright ferroelectric domain possesses a relatively small XMCD asymmetry, consistent with the local magnetization lying approximately perpendicular to the in-plane projection of the incident X-ray beam direction. Therefore discs lying wholly within bright ferroelectric domains are also inferred to be SD, despite the observed spatial variations that arise due to the small signal (in what follows, we will explicitly confirm that bright ferroelectric domains support SD discs). Given that the local magnetization of negative magnetostriction Ni lies perpendicular to the tensile growth strain parallel to the *c* axis [20], we infer that the local magnetization lies perpendicular to the local ferroelectric polarisation in the observed a_1-a_2 domain structure (blue arrows, Fig. 1b).

Next, we used XMCD-PEEM to map the local magnetization in part of a different 10×10 array on the same substrate, both initially (Fig. 2a) and then with 300 V applied (Fig. 2b). These vector maps were constructed from images obtained with the in-plane projection of the incident X-ray beam along two orthogonal directions (green and red arrows, Fig. 2a,b). Both vector maps and their schematic representations (Fig. 2c,d) show that most of these discs are SD. However, at both 0 and 300 V, all discs are grouped in a manner that is reminiscent of Fig. 1, with the magnetic easy axis changing between *x* and *y* on either side of boundaries that lie at 45° degrees to the axes of the disc array. These boundaries therefore reveal the location

of ferroelectric domain walls in the underlying a_1-a_2 domain structure, and even walls lying wholly between discs can be located with good precision given the mark:space ratio of the disc array. On applying 300 V, we see that the ferroelectric domains are only slightly modified, such that most discs experience ±90° rotations of the magnetic easy axis due to piezostrains that do not involve the passage of a ferroelectric wall.

After removing the 300 V, we used MFM to image the entire 10×10 array, and we used optical brirefringence to image the surrounding ferroelectric domains and thus identify the a_1-a_2 structure (Fig. 3a). The extremes of MFM contrast on opposite sides of most discs reveal an intervening SD state, whose orientation decorates the underlying ferroelectric domain. A schematic of Fig. 3a appears in Fig. 4c, where the sign of disc magnetization has been arbitrarily chosen because it was not identified, where data have been omitted for discs in which a SD could not be clearly identified, and where disc colours are only relevant later for the poling experiment described in Fig. 4. The 6×6 array within the red box of Fig. 3a, which is magnified in Fig. 3b and schematized in the 6×6 array at the top-right of Fig. 4c, will now be compared with Fig. 2a,c, in order to explore the consequences of the intervening excursion to 300 V (Fig. 2b,d).

First, we observe (Fig. 3b) that the 300 V excursion has caused each ferroelectric wall to undergo a ~1 μm displacement that wholly traversed one diagonal row of discs (except for the wall shown bottom-right, which started on a disc). Second, we observe that some such discs (identified by green dots in Fig. 3b) have undergone non-volatile ±90° rotations of SD magnetization. Third, we observe that there are other discs (connected by green lines in Figs 2,3) where (1) a SD underwent a ±90° magnetic rotation at 300 V to yield in most cases another SD (Fig. 2), and (2) a subsequent rotation of the same magnitude on removing the voltage yielded in all cases another SD (Fig. 3). The sign of this second rotation determined whether the 300 V excursion resulted in magnetization reversal or no net change, and we assume these outcomes to be non-deterministic. These non-volatile magnetization reversals were identified in spite of the fact that our final state was measured by MFM without sign information, by observing discs in a pairwise fashion: disc pairs connected by a green line in Fig. 2a and Fig. 3b possess opposite magnetizations at the outset, and parallel magnetizations that are collinear with the initial axis of magnetization after having applied and removed the 300 V (this may also be appreciated by comparing the corresponding schematics in Fig. 2c

and the top-right of Fig. 4c). Therefore the application and removal of 300 V caused one member of these paired discs to undergo a non-volatile magnetization reversal, while the other underwent a volatile rotation of magnetization by 90°.

In the first part of our final experiment, we used optical birefringence to image ferroelectric domains in a larger area around the same 10×10 array when poling the sample (Fig. 4). On applying 500 V, the starting a_1-a_2 structure (Fig. 3a) became a single *c* domain (not shown). On then removing the 500 V, we observed the formation and expansion of *a* domains to yield an *a*-*c* structure that became reasonably stable after 30 minutes (Fig. 4a). As expected, the *a*-*c* walls lay at 45° with respect to the a_1-a_2 walls that they replaced. In the second part of our final experiment, an MFM image of the array (Fig. 4b) was taken 24 hours later, permitting us to deduce the final state, which is schematized in Fig. 4d. Note that no SD could be identified in the row lying third from bottom (Fig. 4b), so we have arbitrarily placed the *a*-*c* wall above this row and not below (Fig. 4b,d). Note also that the *a*-*c* wall lying below the top five rows of discs after the 30 minute wait (Fig. 4a) crept up by one row after the 24 hour wait (Fig. 4b,d).

We will now compare the state observed prior to this poling (Fig. 3a) with the state observed after this poling (Fig. 4b) (see also the corresponding schematics in Fig. 4c,d). Our first observation is that poling has much reduced the number of discs in which a SD could be clearly identified (discs without arrows, Fig. 4c,d), primarily because the resulting *a*-*c* domains presented a varied surface topography [24]. Discs in which a SD state could be identified both before and after poling are colour-coded in order to identify any magnetic changes that took place due to the excursion to 500 V. Some of these discs showed non-volatile 90° rotations of magnetization (red and blue discs, Fig. 4d), which may be interpreted in terms of the strain associated with ferroelectric domain switching (yellow, brown and peach domains, Fig. 4d). The rest of these discs underwent no net magnetic change (green discs, Fig. 4d), which is consistent with the fact that they started and finished on *a* domains of unchanged orientation (purple domains, Fig. 4d). Given that each of these unchanged discs is understood to have undergone a ±90° magnetic rotation during the 500 V excursion that produced the ubiquitous *c* domain, we infer that the return to 0 V produced a second rotation of the same magnitude and opposite sign. However, we should assume that this second rotation could have proceeded with either sign, implying that the absence of a net

magnetic change was non-deterministic, and that magnetization reversal could have been observed instead.

Analysis via modelling

From micromagnetic modelling, we find that a magnetic vortex state in the absence of strain (vortex field, Fig. 5) gives way to a SD state (the two SD fields, Fig. 5) in the presence of a sufficiently large uniaxial strain ε_y, whose critical magnitude depends on saturation magnetization M_s. Moreover, if this strain along y is tensile (compressive) then the SD magnetization lies along x (y). Therefore the discs in our virgin sample were rendered SD by a growth strain of critical magnitude or greater, and disc magnetization lay perpendicular to the local polarization in the a_1-a_2 twins given that this growth strain is expected to be tensile and aligned with the c axis [20].

The ME effects seen in discs that did not experience the passage of a ferroelectric domain wall during the excursion to 300 V (Fig. 2,3) arose due to compressive piezoelectric strains of -5×10^{-5} at 300 V, given that $d_{31} = d_{32} = -82$ pm V^{-1} [25]. However, if we assume the bulk Ni value of $M_s = 480$ kA m^{-1} then our observation of SD discs at the outset implies a growth strain of $\geq5\times10^{-4}$ (Fig. 5). This growth strain is one order of magnitude larger than the magnitude of the piezoelectric strains at 300 V, such that the observed magnetoelectric effects would have been precluded. However, a smaller value of $M_s = 230$ kA m^{-1} would permit SD discs to be stabilized by a growth strain that is small enough ($+5\times10^{-5}$) to have been just overcome by the piezoelectric strains at 300 V. This critical value of M_s lies close to the value of 250 kA m^{-1} reported for Ni films that are also 10 nm thick [26-27], but the net value for our discs may well be even smaller due to patterning and oxidation, such that the piezoelectric strains at 300 V exceed rather than match the growth strain. Separately, the ME effects seen in discs that experienced ferroelectric domain switching (Figs 2-4) underwent ~1% changes of strain [9], easily overcoming any plausible value of growth strain, and thus maintaining the SD state after switching.

Conclusions

In summary, we have demonstrated voltage control of magnetization in SD discs of Ni. We observed non-volatile magnetization rotations of 90° due to ferroelectric domain switching (green dots in Fig. 3, red and blue discs in Fig. 4), and non-volatile magnetization reversals due to small and continuous piezoelectric effects (green lines, Fig. 3). These magnetization reversals were non-deterministic, but could be made deterministic if one were to control the magnetization dynamics by driving the magnetic changes with appropriate pulses of strain [28]. This use of small continuous piezoelectric effects is particularly attractive, as it avoids the ferroelectric domain switching that is typically required for ME switching, thus avoiding fatigue.

Acknowledgements. We acknowledge Diamond Light Source for time on beamline I06 under proposal SI9590, and Grant No. F/09 154/E from the Leverhulme Trust. X. M. is grateful for support from the Royal Society.

Fig. 1. Ni discs on a BTO substrate. (a) Schematic showing three capped Ni discs on a metallized BTO substrate. (b) XMCD-PEEM image of Ni discs combined with an XLD-PEEM image of their BTO substrate (20 μm-diameter field of view, green arrow represents in-plane projection of incident beam direction). For each ferroelectric domain, double-headed arrows show without sign the orientations of ferroelectric polarization **P** (blue) and local magnetization **M** (red).

Fig. 2. Voltage-driven 90° magnetic rotations in Ni discs on a BTO substrate. (a,b) XMCD-PEEM vector maps and (c,d) schematics showing Ni disc magnetizations (black arrows) with (a,c) 0 V and (b,d) 300 V applied across the substrate (15 μm × 15 μm field of view, green and red arrows represent in-plane projections of incident beam directions). In (d), disc colours describe the magnetic changes that arose due to the 300 V piezostrains that are also colour-coded. In (c,d), blue lines denote ferroelectric domain walls, and double-headed blue arrows show without sign the inferred orientations of ferroelectric polarization. In (a,c), green lines pair discs in order to identify magnetization reversals in one pair member on returning to 0 V as shown in Fig. 3. Data for discs on the same substrate used for Fig. 1.

Fig. 3. Subsequent imaging after voltage removal. After removing the 300 V from the sample used for Fig. 2, we show (a) an MFM image of the same Ni discs (inside red square) and others, superimposed on an optical image of the surrounding BTO domains. A schematic of (a) appears in Fig. 4c. (b) Magnified view inside the red square of (a), with adjacent schematic. For each ferroelectric domain (dark or pale), double-headed arrows show the orientations without sign of ferroelectric polarization **P** (blue) and local magnetization **M** (red). Blue lines copied from Fig. 2c represent ferroelectric domain walls before the 300 V was applied and removed. The ferroelectric domain walls observed here on returning to 0 V have passed (single-headed blue arrows) under discs that are marked with a green spot if they consequently underwent non-volatile 90° rotations of SD magnetization. Green lines in (b) are copied from Fig. 2a,c in order to identify magnetization reversals in one pair member due to the 300 V excursion in Fig. 2.

Fig. 4. Non-volatile 90° rotations after poling with a larger voltage. After subsequently applying and removing 500 V across the sample used for Fig. 3, we show (a) an optical image of the same Ni discs and the surrounding domains in BTO (large white triangles are

lithography markers), and (b) an MFM image of the same discs taken 24 hours later. Schematics of the sample (c) before poling (data from Fig. 3a), and (d) 24 hours after poling (data from b). Blue lines denote ferroelectric domain walls, double-headed blue arrows show the orientations without sign of ferroelectric polarization **P**. For discs identified to be SD in both (c) and (d), the colours in (d) describe the changes in both disc magnetization (black arrows) and local strain.

Fig. 5. Phase diagram of strained Ni discs. The magnetic ground state depends on saturation magnetization and strain (M_s,ε_y). Magnetic maps representing the SD states at (480 kA m^{-1}, $\pm 5\times10^{-4}$) and the vortex state at (480 kA m^{-1}, 0) are presented using the colour wheel and arrows to identify the direction of local magnetization. Disc diameter 1 μm, thickness 10 nm.

References

[1] Mathur N D 2008 *Nature* **591** 454

[2] Nan C W, Bichurin M I, Dong S, Viehland D and Srinivasan G 2008 *J. Appl. Phys.* **103** 031101

[3] Hu J *et al.* 2017 *npj Computational Materials* **18** 3

[4] Wang Y *et al.* 2010 *NPG Asia Materials* **2** 61

[5] Heron J T, Schlom D G and Ramesh R 2014 *Applied Physics Reviews* **1** 021303

[6] Lahtinen T H E, Franke K J A and van Dijken S 2012 *Sci. Rep.* **2** 1

[7] Geprägs S *et al.* 2010 *Appl. Phys. Lett.* **96** 142509

[8] Skumryev V *et al.* 2011 *Phys. Rev. Lett.* **106** 1

[9] Ghidini M *et al.* 2015 *Adv. Mater.* **27** 1460

[10] Wu T *et al.* 2011 *J. Appl. Phys.* **109** 7

[11] Sahoo *et al.* 2007 Phys. Rev. B **76** 092108

[12] Lei N *et al.* 2013 *Nat. Commun*. **4** 1378

[13] Hu J *et al*. 2011 *Nat. Commun.* **2** 553

[14] Hubert A and Schäfer R *Magnetic Domains,* Springer-Verlag, Berlin, Germany, 1998.

[15] Parkes D E *et al.* 2014 *Appl. Phys. Lett.* **105** 062405

[16] Li Q, Tan A, Scholl A, Young A T, Yang M, Hwang C, N'Diaye A T, Arenholz E, Li J and Qiu Z Q 2017 *Appl. Phys. Lett.* **110** 262405

[17] Beardsley R P, Bowe S, Parkes D E, Reardon C, Edmonds K W, Gallagher B L, Cavill S A and Rushforth A W 2017 *Scientific Reports* **7** 7613

[18] Buzzi M, Chopdekar R V, Hockel J L, Bur A, Wu T, Pilet N, Warnicke P, Carman G P, Heyderman L J and Nolting F 2013 *Phys Rev. Lett.* **111** 027204

[19] Wren *et al.* 2015 *J. Appl. Phys.* **118** 023906

[20] Lahtinen T H E, Tuomi J O, van Dijken S 2011 *Adv. Mater.* **23** 3187

[21] Necas D and Klapetek P 2012 *Cent. Eur. J. Phys.* **10** 181

[22] Vansteenkiste A, Leliaert J, Dvornik M, Helsen M, Garcia-Sanchez F and Van Waeyenberge B 2014 *AIP Advances* **4** 107133

[23] Michels A, Weissmüller J, Wiedenmann A and Barker J G 2000 *J. Appl. Phys.* **87** 5953

[24] Kalinin S V and Bonnell D A 2000 *J. Appl. Phys.* **87** 3950

[25] Tazaki R, Fu D, Itoh M, Daimon M, Koshihara S-Y 2009 *J. Phys.: Condens. Matter* **21** 215903

[26] Coren R and Juretschke H J 1957 *J. Appl. Phys.* **28** 806

[27] Wedler G and Schneck H 1977 *Thin Solid Films* **47** 147

[28] Ghidini M *et al.* 2013 *Nat. Commun.* **4** 1453

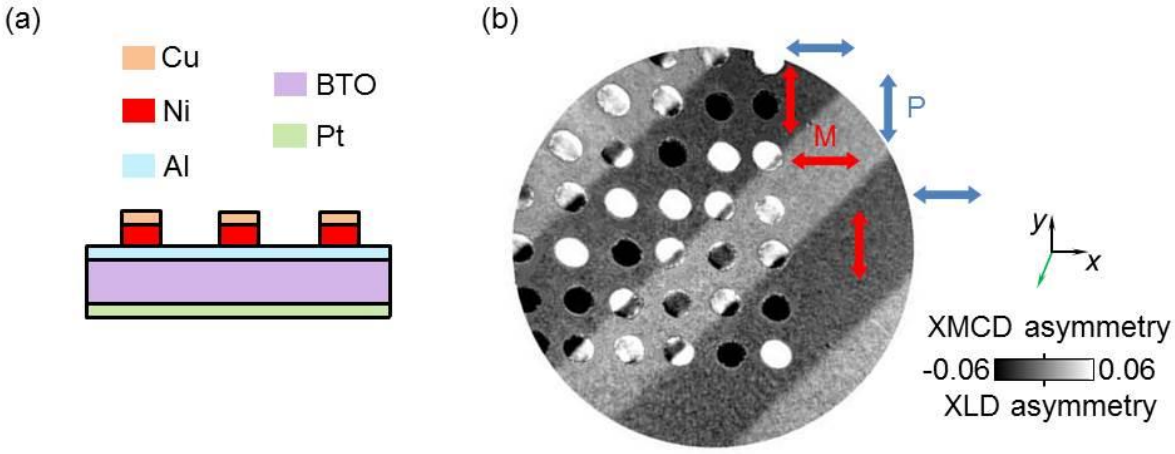

Fig. 1

Fig. 2

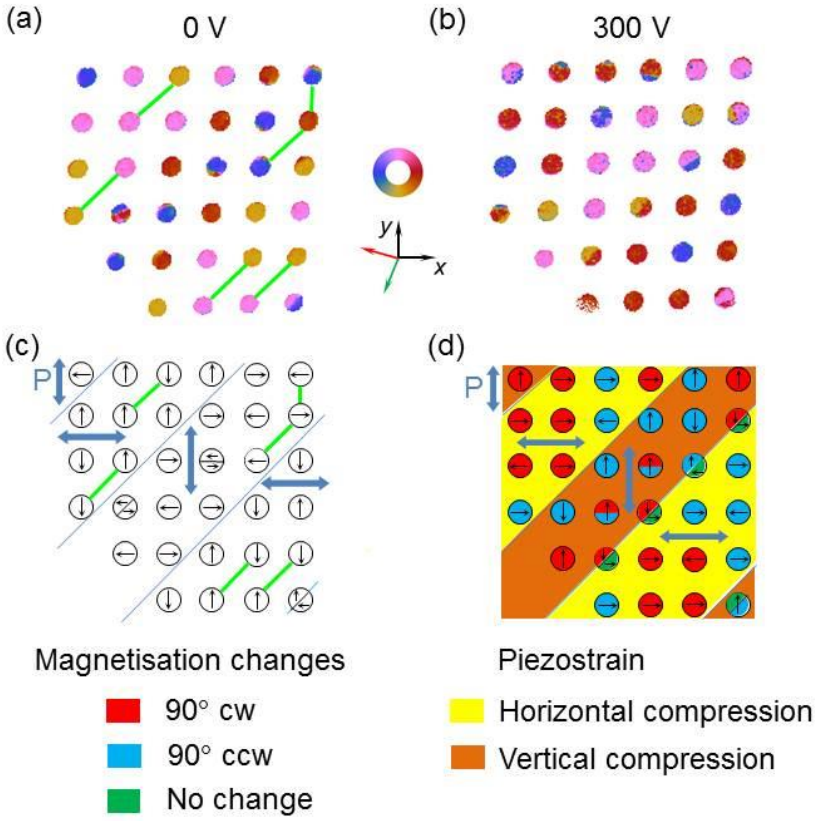
(a)
0 V
(b)
300 V
y
x
(c)
P
(d)
P
Magnetisation changes
90° cw
90° ccw
No change
Piezostrain
Horizontal compression
Vertical compression

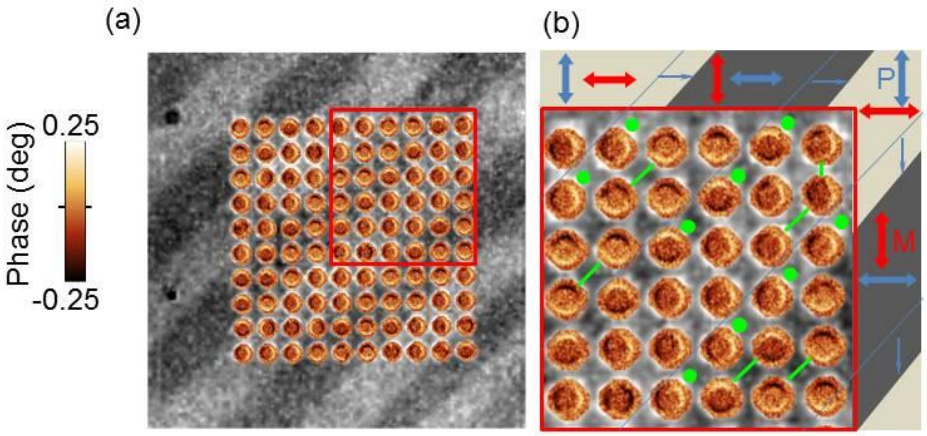

Fig. 3

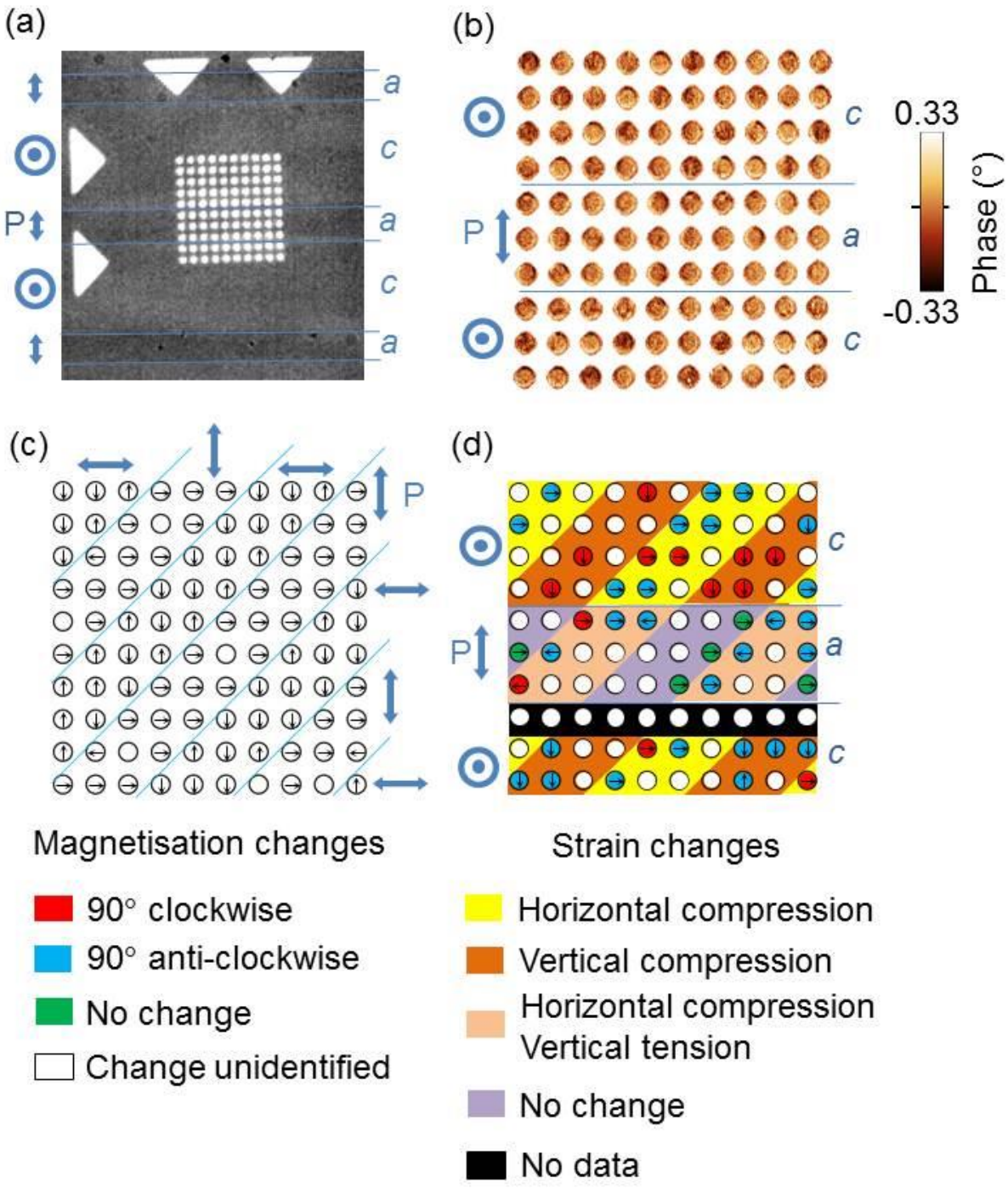
(a)
a
c
P
a
c
a
(b)
c
P
a
c
0.33
-0.33
Phase (°)
(c)
P
(d)
c
P
a
c
Magnetisation changes
90° clockwise
90° anti-clockwise
No change
Change unidentified
Strain changes
Horizontal compression
Vertical compression
Horizontal compression
Vertical tension
No change
No data

Fig. 4

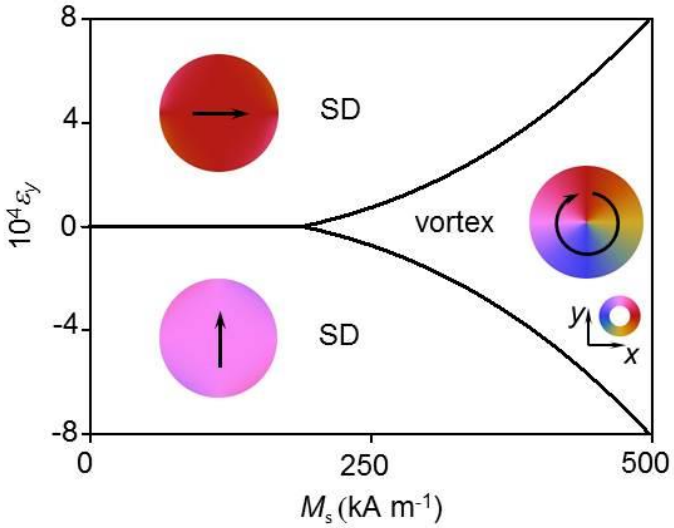

Fig. 5